A volumetric method for measuring the longitudinal arch of human tracks and feet

Kevin G. Hatala[1], Stephen M. Gatesy[2], Armita R. Manafzadeh[3,2], Elizabeth M. Lusardi[1], Peter L. Falkingham[4]

[1]Department of Biology, Chatham University, [2]Department of Ecology, Evolution, and Organismal Biology, Brown University, [3]Institute for Biospheric Studies, Yale University, [4]School of Biological and Environmental Sciences, Liverpool John Moores University

ABSTRACT

Fossil footprints (i.e., tracks) were believed to document arch anatomical evolution, although our recent work has shown that track arches record foot kinematics instead. Analyses of track arches can thereby inform the evolution of human locomotion, although quantifying this 3-D aspect of track morphology is difficult. Here, we present a volumetric method for measuring the arches of 3-D models of human tracks and feet, using both Autodesk Maya and Blender software. The method involves generation of a 3-D object that represents the space beneath the longitudinal arch, and measurement of that arch object's geometry and spatial orientation. We provide relevant tools and guidance for users to apply this technique to their own data. We present three case studies to demonstrate potential applications. These include, (1) measuring the arches of static and dynamic human feet, (2) comparing the arches of human tracks with the arches of the feet that made them, and (3) direct comparisons of human track and foot arch morphology throughout simulated track formation. The volumetric measurement tool proved robust for measuring 3-D models of human tracks and feet, in static and dynamic contexts. This tool enables researchers to quantitatively compare arches of fossil hominin tracks, in order to derive biomechanical interpretations from them, and/or offers a different approach for quantifying foot morphology in living humans

KEYWORDS

Longitudinal arch, fossil footprints, tracks

INTRODUCTION

The evolution of arched feet

For at least the past century, paleoanthropologists and comparative anatomists have allocated significant attention to studying the emergence and evolution of our foot's longitudinally arched morphology (Morton, 1924). Humans are the only extant primate with this foot anatomy, so it has been assumed that it must be uniquely well suited for locomotor functions. Recent studies have reshaped our understandings of whether and how the longitudinally arched configuration of our foot skeleton actually contributes to the demands of human bipedalism, and of which aspects of foot anatomy enable functions typically attributed to the longitudinal arch (e.g., Kelly et al., 2014, 2015; Venkadesan et al., 2020; Welte et al., 2018, 2021; Holowka et al., 2021). Still others have proposed that a longitudinally arched foot may be

more important for facilitating foot function during running than during walking (e.g., Stearne et al., 2016; Holowka & Lieberman, 2018).

It is very difficult, however, to understand longitudinal arch anatomy from skeletal fossils. Part of that difficulty stems from the fact that the arch is supported by several soft tissue elements, which do not typically fossilize. The bones that do fossilize are often fragmentary or found in isolation. Some researchers have hypothesized arch anatomies for fossil hominins based on just one or two bones, but others who have analyzed those very same elements have found conflicting results (DeSilva & Throckmorton, 2010; Ward et al., 2011; Drapeau & Harmon, 2013; Prang, 2015).

Fossil footprints (i.e., tracks) have been viewed as a potentially more viable path for reconstructing arch morphology. Tracks preserve records of the complete, articulated feet of fossil hominins during life. Their longitudinally arched shapes have been interpreted as direct images of plantar foot anatomy, and assumed to record longitudinally arched foot anatomies in early hominins from the Pliocene and early Pleistocene (Leakey & Hay, 1979; Day & Wickens, 1980; Bennett et al., 2009). More recent work has demonstrated that the longitudinal arches of footprints are rarely accurate records of foot anatomy, and that they instead represent an important record of foot kinematics (Hatala et al., 2023). Thus, arched footprints remain uniquely valuable for understanding the evolution of human locomotor kinematics.

Methods for quantifying arch morphology

A variety of techniques for quantifying longitudinal arch morphology in living human feet have been developed for primarily clinical or sutorial purposes. The absolute or relative height of the medial longitudinal arch can be measured directly, using a variety of two-dimensional linear or angular measures (e.g., Williams & McClay, 2000). More recently, with the growth and availability of 3-D scanning technology, direct 3-D measurements have become more common. These methods extend beyond point-to-point measurements, and have recently included statistical shape modeling to describe complete foot anatomy and variation, including that of the longitudinal arch (e.g., Stanković et al., 2018; Schuster et al., 2021).

Aside from direct foot measurement, clinicians and footwear designers have, for over a century, evaluated what they refer to as “footprints” to assess longitudinal arch morphology (McKenzie, 1909). Here, “footprints” are acquired by coating the plantar surface of a foot with paint or ink, and asking a person to walk or stand on paper to quantify how much of the foot contacted the ground. The exact nature of these measurements has changed over time, but most have focused on quantifying the 2-D area of foot contact beneath the longitudinal arch (i.e., the instep; for a brief review see Cavanagh & Rodgers, 1987). More recently, similar methods have also been applied to measure high-resolution 3-D foot scans (Domjanic et al., 2015).

Fossil footprints (i.e., tracks) differ fundamentally from paint/ink prints, because they represent a 3-D record of a complex interaction in which the foot and substrate mutually moved and deformed. Many of the tracks known from the human fossil record are deep impressions that were formed as hominins walked through soft, deformable substrates. In a deep track, the foot sinks to the point where the entire plantar surface contacts and deforms the ground. In these cases envisioning the 3-D track as a 2-D paint mark is difficult if not impossible, as it is unclear where on the track’s continuous 3-D topography one could objectively designate

borders to define a 2-D plantar foot outline. Historically, the presence/absence or the height of arches within hominin tracks have usually been discussed in qualitative or relative terms (e.g., appearing higher or lower than in other hominin tracks or modern human tracks) because there is no easy way to measure them directly. For example, the height of the navicular is impossible to identify with confidence, as the bone does not leave behind any clear landmark within track morphology. Given the lack of appropriate methods for measuring track arches, some have attempted the same types of measurements described above for paint-on-floor traces (Bennett et al., 2009). However, we do not believe that methods designed to measure the instep of paint prints can be applied directly to 3-D tracks, given the fundamental differences between the two types of records and the mechanics of how they form.

Again, our recent biplanar X-ray experiments have revealed that the longitudinal arch of a track is shaped by the flow of sediment in response to foot kinematics, and does not accurately represent the longitudinal arch anatomy of the foot that created it (Hatala et al., 2018, 2021, 2023). Still, even though the longitudinal arch of a track is not a direct anatomical signal, quantification of this feature offers important evidence for understanding the evolution of hominin foot kinematics (Hatala et al., 2023).

A new, volumetric method for quantifying the arches of tracks and feet

Here, we present a new, 3-D volumetric approach that we developed for quantifying and comparing the longitudinal arches of tracks. This technique can also be applied to measure longitudinal arches from 3-D scans of human feet. In fact, we have applied the technique to measure and compare the arches of tracks with the arches of the feet that made them (Hatala et al., 2023). We note that we have slightly adjusted our calculations since our first presentation of this measurement technique (Hatala et al., 2023). The new calculations do not change any of the results or conclusions from that prior publication. We found that the revised formula merely helps with applications of the measurement tool to marginal cases (i.e., tracks that are much shallower or much deeper than those we analyzed previously). We present the approach in detail, and we provide all of the relevant software tools, such that others can implement similar measurements in their own studies of hominin tracks or feet.

MATERIALS & METHODS

Overview of the Method

Our approach is based on polygonal track and foot models that could be derived from a variety of sources, such as photogrammetry, scanning (laser, structured light, CT), animation, or simulation. We sample the volume of space below the track/foot arch using a prism consisting of parallel base and roof triangles connected by three perpendicular walls (Fig.1). The user interactively reshapes and positions the prism by registering virtual markers representing its base vertices at the center of the heel impression, and at the approximate positions of the first and fifth metatarsophalangeal joints. Wall height of the prism is then adjusted to ensure that the prism fully captures the arch. Calculating the Boolean intersection between a track/foot and a prism model yields an arch model (Fig. 1B,C), from which relative arch volume (RAV) and other

parameters are derived (Table 1). Detailed instructions and links to scripts for implementation in Autodesk Maya and Blender are presented in Appendix 1 and Appendix 2.

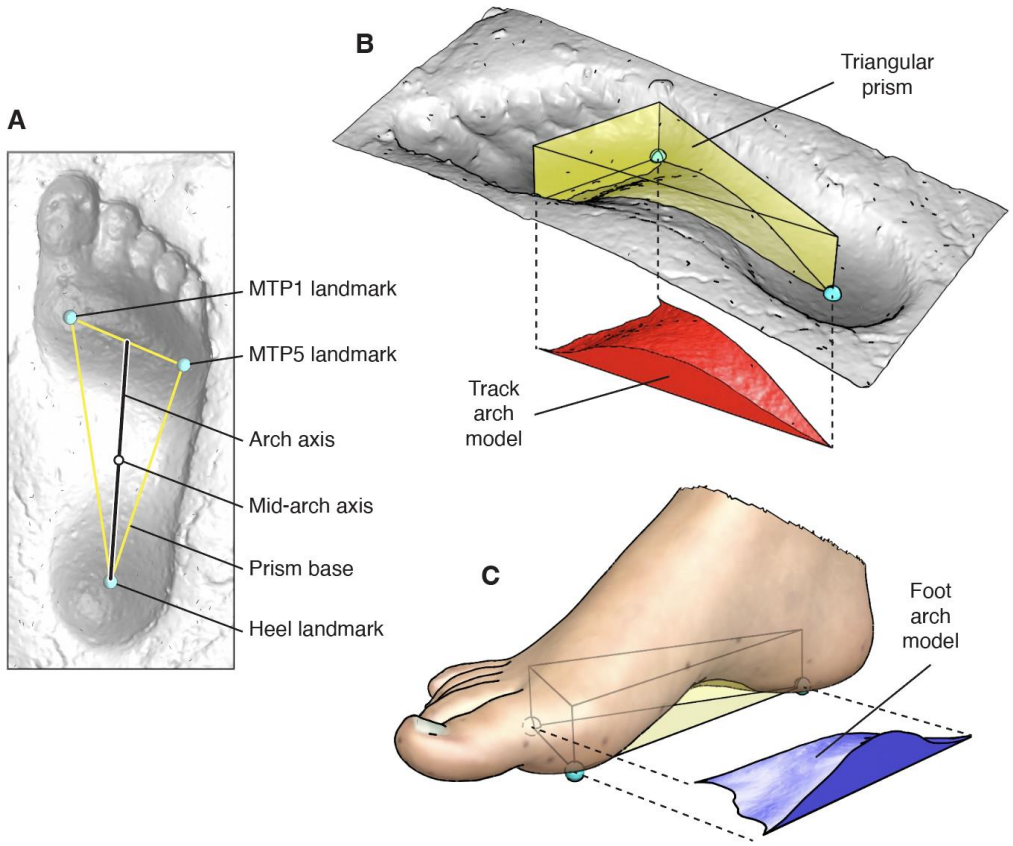

Fig. 1. Boolean intersection between a triangular prism and a track/foot model yields an arch model. (A) Three landmarks (aqua spheres) designate the prism's base. (B) A track arch model (red) samples the volume between landmarks and the deformed substrate. (C) A comparable foot arch model can be derived from static or dynamic plantar anatomy.

RAV was developed to measure both the concavity of a foot's anatomical arch, as well as the convexity of a track's corresponding morphology. Intuition about the meaning of specific RAV values is hampered by the triangular nature of the sampling geometry, but some examples can help. A RAV of 100 designates the volume of any completely filled prism having a wall height equal to the ⅔ root of its base area. A RAV of 25 is equivalent to an arch volume filling only one quarter of such a prism, a RAV of 10 filling one tenth, and so on. Thus, RAV represents the average height of the arch object relative to the area of its base, expressed as a percentage.

To help compare arch variables among hominin tracks that differ in absolute size (i.e., outline dimensions) and also in depth, we calculated relative depth. To do this, an arch axis was

defined, spanning from the heel landmark to the midpoint of another axis drawn between the two metatarsophalangeal joint markers (Fig. 1A). The absolute depth of the arch axis midpoint is measured, and is then divided by the arch axis length. Relative depth provides an important measure of how much substrate was displaced relative to the hominin's foot size. We have seen previously that the RAVs of human tracks tend to increase as relative depth increases, and we have observed a logarithmic relationship between the two variables (Hatala et al., 2023). In other words, the same subject can produce tracks of different RAV, depending on how much substrate they displace when forming a given track. We expect that other aspects of track morphology vary with relative depth as well, because depth-related trends have been observed across multiple studies (e.g., Bennett & Morse, 2014; Morse et al., 2013).

Table 1. Arch variables measured in Maya and Blender scripts.

Variable	Description
Relative arch volume (RAV)	Arch volume, divided by ⅔ root of base area, expressed as a percentage
Relative depth	Mid-axis depth, divided by axis length
Pitch	Pitch of arch axis, measured in degrees (heel deeper than forefoot results in positive pitch)
Roll	Roll of metatarsophalangeal joint axis about arch axis, measured in degrees (external rotation of metatarsophalangeal joint axis results in positive roll)
Arch volume	Volume of arch model, measured in cm^3
Base area	Area of prism base, measured in cm^2
Axis length	Length from heel marker to middle of metatarsophalangeal joint axis, measured in cm
Mid-axis depth	Depth of arch axis at its midpoint, measured in cm

Side	Indicates whether the selected object was designated as a right or left foot or track

Case studies implementing volumetric arch measurement

Here we provide three case studies of RAV implementation, using data collected during recently published experiments (Hatala et al., 2018; 2021; 2023). Full details of experimental protocols are available in those references, and are summarized briefly here.

In these experiments, between 85 and 115 lead beads 1.5 mm in diameter (with sticker backings) were affixed to subjects' right feet using medical adhesive. Prior to their attachment, a template of bead locations was drawn on their foot using a semi-permanent marker, and each subject's foot was 3-D scanned using a structured light scanner. After scanning was complete, the lead beads were fixed to the marker locations. With beads attached to their feet, subjects stood or walked upon a variety of substrates for a minimum of 13 trials each captured by biplanar X-ray video at 50 frames per second. For the first trial, each subject quietly stood in the field of biplanar X-ray view, and we captured an image of their static, weight-bearing foot. For at least three trials subjects walked at self-selected comfortable walking speeds across a rigid carbon fiber plank. For at least nine more trials, subjects walked at the same self-selected speeds across three muds of increasing compliance (minimum three trials per substrate). For mud trials, the footprints left behind were captured to render 3-D models using photogrammetry or a structured light scanner.

Following acquisition of experimental data, bead 3-D positions were tracked using XMALab software. Each subject's 3-D foot scan was imported to Autodesk Maya, and the tracked 3-D bead positions were used to animate their 3-D foot model as it moved and deformed within the calibrated biplanar X-ray space. These 3-D animations enabled visualization and direct quantification of foot motion and deformation throughout foot-substrate interactions in each trial.

Measuring arches of static and dynamic feet

In our first application, we measured the longitudinal arches of human feet under static and dynamic conditions. Using two forms of static data, we compared the same subjects' feet in unloaded and weight-bearing conditions. To do so, we first measured the 3-D foot scan models that were collected prior to bead attachment, while subjects rested their leg upon a stool. We then measured the animated 3-D foot models during static, quiet standing trials. As described above, deformations of the foot scan models were dictated by the real 3-D bead location data acquired with biplanar X-ray. Measurements under these two conditions allowed us to evaluate the extent and nature of arch deformation that was induced by weight-bearing.

Next, we quantified dynamic frame-by-frame arch morphology as the same subjects walked across solid and deformable substrates. These quantifications relied upon frame-by-frame measurement of the 3-D animated foot in each trial. Using Autodesk Maya's "Create animation snapshot" tool, we output .obj models of the animated foot's pose at each observed data frame. These models were then directly measurable in the same way as any other static 3-D foot model. By computing arch variables across multiple trials, we could compare temporal patterns of arch deformation during walking on different substrates.

Comparing foot arches to track arches

In a second application, which was also presented in one of our recent publications (Hatala et al., 2023), we compared the arches of tracks to the arches of the feet that created those tracks. For the latter, we measured arch morphology at midstance while the track was being created. The midstance measurements provided us with another "anatomical" measurement that might vary depending on whether and how a given deformable substrate supported the arch (i.e., impeded vertical arch deformation) while the foot moved through it. This allowed us to evaluate the extent to which the longitudinal arches of tracks resembled the longitudinal arches of the feet that created them.

Comparing dynamic foot arches to dynamic track arches

Finally, in a third application that was also presented in a recent publication (Hatala et al., 2023), we took dynamic (frame-by-frame) volumetric arch measurements from both feet and tracks, throughout track creation. This was possible using DEM simulations of substrates deforming in response to foot motions that were captured during *in vivo* experiments. We have previously demonstrated that these simulations very closely match observed reality, and offer valuable tools for understanding how track morphology develops (Falkingham and Gatesy, 2014; Falkingham et al., 2020; Hatala et al., 2021). Simultaneous visualization and quantification of feet and tracks allowed us to understand the process that causes track arches to differ morphologically from the arches of the feet that created them (Hatala et al., 2023). Here we highlight the application of volumetric arch measurement tools in order to pinpoint how and why foot and track arches diverge.

RESULTS

Case studies implementing volumetric arch measurement

Measuring arches of static and dynamic feet

Comparisons of arch volumes from unloaded and weight-bearing feet showed that RAV decreases substantially under the weight-bearing conditions (Table 2). Unloaded foot RAVs ranged from 6.83 to 8.89, while weight-bearing RAVs ranged from 0.84 to 3.00. Within subjects, RAV decreased by between 66.27% and 87.68% during weight-bearing when compared with unloaded conditions.

Table 2. Arches of unloaded and weight-bearing feet in four human subjects.

Subject	Unloaded RAV	Weight-bearing RAV	% change due to weight-bearing
1	8.89	3.00	66.27

2	6.83	0.84	87.68
3	7.69	1.52	80.18
4	6.94	1.32	80.96

For dynamic foot analyses, we selected four variables available from our volumetric measurement tool - RAV, pitch, roll, and mid-axis length - and we observed how those aspects of arch morphology changed throughout stance phase while walking on each of four different substrates (rigid carbon fiber and three muds of increasing compliance). We present data from a single subject here, for simple demonstration of this application of the arch measurement tool.

The pattern of RAV over time was very similar when the same subject walked on rigid carbon fiber and on firm mud (Fig. 2A). When they walked on softer muds that were 2.5 and 5 cm deep (labeled “wet 2.5” and “wet 5” in Fig. 2), RAV remained relatively higher in the early parts of stance phase, before dropping and following patterns similar to those observed on the two firmer substrates from approximately 70% of stance phase onward (Fig. 2A). These observations suggest that arch motion and deformation patterns differ earlier in stance phase across different substrates, but that they converge on a common trajectory while generating propulsive forces later in stance.

Measurements of pitch over time were quite similar across substrates (Fig. 2B). In each trial, pitch started out as positive (toes up), stabilized to some extent at an angle close to zero (foot flat), and then switched to negative during the propulsive part of stance phase (toes down). Slight variations were apparent, however. When walking on carbon fiber, the subject unsurprisingly experienced a prolonged period of near-zero pitch while the foot was flat on the solid surface. In muds, the heel rose and the forefoot sunk earlier in stance phase. In the deepest mud (“wet 5”), the foot’s pitch never appeared to reach a stable, flat position (Fig. 2B). There was even a slight increase in pitch in the earliest part of stance on deep mud, when soon after heel strike the heel sunk at a faster rate than the rest of the foot. This did not occur on any of the more stable substrates.

The patterns by which the arch lengthened during stance phase were similar across all substrates (Fig. 2C), which was surprising given the differences observed in all of the other measurements. The arch lengthened early in stance phase (roughly 0-20% stance phase), stabilized during an intermediate window of time (about 20-55%), then lengthened again (55-80%) before rapidly shortening late in propulsion (80% onwards). This subject’s arch appeared longer on firm mud than on any other substrate, although it still followed the same temporal pattern that was observed on the others. The scale of distance between the lines is quite small (~1.5 mm; equivalent to one bead diameter), however, so we do not make much of this difference. On the deepest mud (“wet 5”) arch length began its secondary increase earlier than on any of the other substrates (~45% stance phase; Fig. 2C). As with pitch, we attribute this to

the lack of stability on this substrate compared with the others, which causes the foot to continue rotating throughout stance rather than finding a true “foot flat” position.

Measurements of roll over time were similar across three of the four substrates, with the deepest mud again being the outlier (Fig. 2D). The forefoot everted relative to the hindfoot (roll increases) soon after foot contact, and then leveled out or stabilized once the foot was flat. Roll then increased continuously throughout push-off. On the deepest mud, roll started low and then increased continuously throughout stance phase, never reaching a stable plateau. This may be attributed to this deepest and most pliable mud conceding to the foot’s motions rather than resisting them.

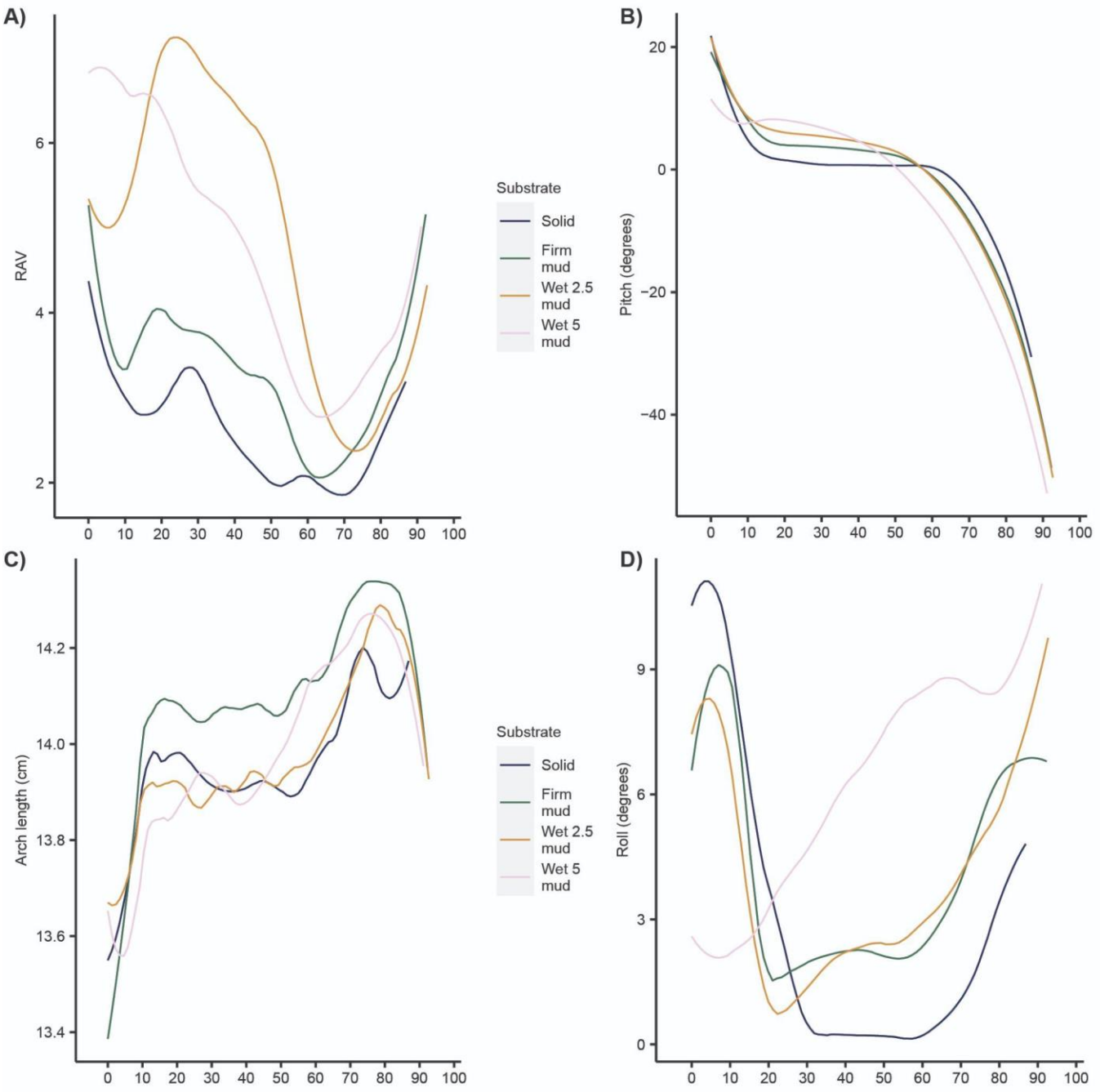

Fig. 2. Measurements of foot arches during walking on different substrates. A subset of arch model measurements - RAV (A), pitch (B), arch length (axis length; C), and roll (D) - were calculated from frame-by-frame poses of a subject's 3-D animated foot as they walked across four different substrates. The x-axes are converted to percentages of stance phase (0-100%) for ease of comparison across trials that differ in absolute duration.

Comparing foot arches to track arches

By measuring the arch of the foot at midstance and then the arch of the track that was formed in each trial, we directly compared the foot's anatomical arch to the arch of the track that

the foot left behind. In firm mud, track RAV measurements appear to match closely the RAV measured from feet at midstance (Fig. 3). However, we believe this is more coincidental than mechanistically linked - from our video recordings we observed that the plantar surface beneath the longitudinal arch often did not completely contact the substrate. The track ended up with a RAV similar to the foot because the substrate was displaced during heel strike and toe-off, not because the substrate generated a “mold” of foot anatomy.

In deeper muds, which more closely resemble most known tracks from the human fossil record, track RAV measurements further diverge from those of the feet that created them. In 2.5 cm deep mud (“wet 2.5”) track RAV can be two to three times larger than foot RAV; in 5 cm deep mud (“wet 5”) tracks can have RAV measurements three to five times larger than the feet that made them (Fig. 3). This result emphasizes the mismatch between the arches of tracks and the arch anatomy of the feet that made them. As we have shown elsewhere, track arches reflect kinematic signals rather than anatomical ones (Hatala et al., 2023).

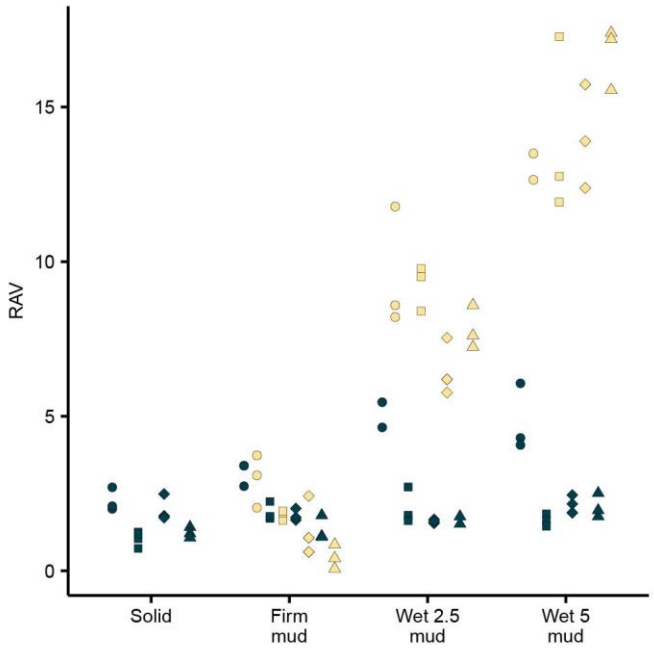

Fig. 3. Arches of tracks and the feet that produced them. Foot arches (dark green) were measured from 3-D animated feet at mid-stance in each trial. Track arches (yellow) were measured from 3-D models of the footprints produced in those same trials. The four symbols correspond to four subjects whose data were analyzed here.

Comparing dynamic foot arches to dynamic track arches

By extracting data from particle simulations, our arch measurement tool can also be used to study simultaneous changes to foot and track arches over time (Fig. 4). This has allowed us to identify when and how track RAV comes to misrepresent foot RAV, and was essential for determining that track RAV represents a kinematic signal rather than an anatomical one (Hatala et al., 2023).

Track RAV diverges from foot RAV starting just before 50% of stance phase (Fig. 4), increasing sharply while foot RAV is instead decreasing. At this time, we can see that the heel is

lifting from the substrate. The foot rotates over top of the substrate beneath its longitudinal arch, as the forefoot sinks deeper into the mud. The space that was occupied by the heel and the proximal part of the arch offers a vacant space where substrate can also be pushed backwards and upwards by the forefoot when it exerts propulsive forces (Fig. 4). In this way, arch morphology ends up being shaped by the foot's continuous motion as it navigates the deformable substrate, rather than representing a snapshot of static foot anatomy.

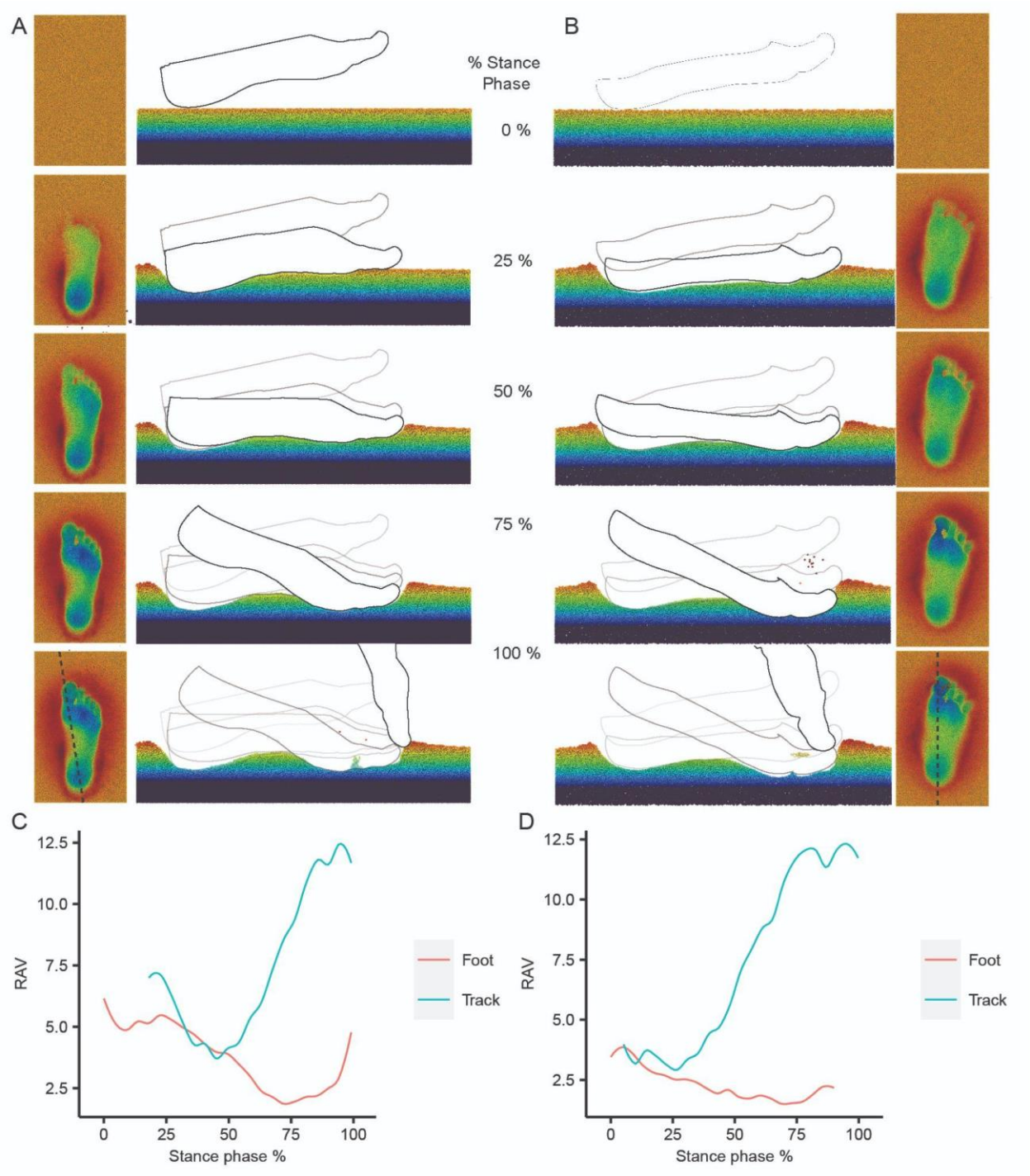

Fig. 4. Discrete Element Method (DEM) simulations showing the pattern by which track arches are formed. Subjects with relatively higher (A) and relatively lower arched feet (B) produce tracks with similar longitudinal arches (similar RAV) because of the ways their feet move through the deformable substrate. Measurements throughout track simulation show that the arches of tracks sharply diverge from the arches of the feet that made them by about 50% stance phase (C, D).

DISCUSSION

The case studies presented here demonstrate multiple applications of our volumetric arch measurement tool for quantifying the longitudinal arches of human tracks and human feet. We developed the method with a primary interest in the longitudinal arches of tracks – we wanted to quantify this aspect of 3-D track morphology, which was long considered important but remained difficult to measure. At the same time, we transferred the method to measure 3-D surface models of human feet, in order to test the hypothesis that a track's longitudinal arch resembles the plantar shape of the foot that created it. In contexts where researchers' sole objective is an anatomical measure of longitudinal arch height perhaps other, skeletally-based measurements are more appropriate (e.g., Williams & McClay, 2000). That said, given the increasing use of 3-D foot scanners to evaluate arch morphology in living humans (e.g., Schuster et al., 2021; Stanković et al., 2018), perhaps our volumetric method (or derivations of it) can be useful for clinical assessments or in footwear design.

The small sample sizes of our case studies mean that we cannot draw generalized conclusions about arch anatomy in modern humans, but we can offer some comparisons with other measurement techniques. Looking first at our static foot measurements in unloaded and weight-bearing conditions (Table 2), we detected percentage decreases in RAV that far exceed some of those observed using 2-dimensional linear and angular arch measurements. For example, Tsung et al. (2003) observed that arch height was about 20% lower, on average, during weight-bearing compared with non-weight-bearing conditions. Williams and McClay (2000) observed even smaller differences (e.g., decreases of 13% for navicular height, and 8% for height of dorsum of foot/truncated foot length) when comparing arch height in 10% and 90% weight-bearing conditions. We observed RAV decreases between 66 and 88%, but perhaps this dramatic difference is not surprising given the contrast between our method and those employed in the other studies. Measuring volumetric changes on the plantar surface of the foot means that our technique will capture external morphological changes that are not captured by, and may have little effect on, linear measurements between the ground and the navicular, or between the ground top of the foot. Again, we do not contend that our method is more accurate or more appropriate for all anatomical or functional studies, only that it captures the most relevant information for studying the relationships between tracks and plantar morphology.

Our dynamic arch measurements also afford some opportunities for comparisons with other studies. There have been very few studies of arch deformation on deformable substrates, but Holowka et al. (2018) measured arch deformation on solid substrates in a study of foot stiffness in habitually shod and unshod humans. The dynamic patterns that they observed in longitudinal arch angle and in changes to longitudinal arch height (Holowka et al., 2018 [Fig. 3]), match well with the patterns that we observed in arch length and RAV, respectively, during locomotion on solid substrates (Fig. 2). The similarity of these temporal patterns suggests that

even if our volumetric arch measurements differ from linear measures in absolute terms, they still capture similar patterns of dynamic changes during locomotion.

As described before, we initially developed this volumetric arch measurement tool in order to directly compare the arches of tracks to the arches of the feet that made them. We first observed that the morphologies of track arches, particularly those made in deep mud, did not match well with direct measurements of the arches of the feet that made them (Fig. 3). Using the Discrete Element Method (DEM) (Kloss & Goniva, 2011; Stukowski, 2010) we conducted experimental data-driven simulations of track formation (Hatala et al., 2021) to examine the foot-substrate interactions that generated the longitudinal arches of tracks. From these simulations, we understood that track arches form as a consequence of the foot's heel-sole-toe rollover pattern occurring in a deformable substrate (Fig. 4). Thus, a track's arch is a kinematic signal and not an anatomical one (Hatala et al., 2023).

Differences between track and foot arch anatomy are amplified as track depth increases (Fig. 3), and most of the known Plio-Pleistocene fossil tracks (e.g., those from Laetoli, Tanzania (Leakey & Hay, 1979) and Ileret, Kenya (Bennett et al., 2009)), are sufficiently deep that we expect substantial differences between track and foot arch anatomy. Some fossil track surfaces actually provide data that directly demonstrate that the same individual can produce differently arched tracks, depending on substrate compliance. At Walvis Bay, Namibia, Morse et al. (2013) described substrate-driven differences in track morphology that were observed within trackways produced by the same individuals. In our recent study (Hatala et al., 2023), we also found that the RAVs of tracks made by the same individuals increased with relative depth. Because track arches are kinematic signals, and foot kinematics change across substrates of different compliance, the same individuals produce differently arched tracks in different localized substrate conditions (see also Fig. 3).

One application not covered here is the comparative analysis of fossil hominin tracks. For such applications we refer the reader to a recent study in which we carried out such analyses (Hatala et al., 2023). However, we wish to draw further attention to one caveat that was described in that study. There we cautioned against blind application of this volumetric arch measurement tool to non-hominin tracks, and against the assumption that it will continue to provide results with similar meaning. In that study (Hatala et al., 2023) we applied this volumetric measurement technique to chimpanzee tracks, and we showed that arch model geometry is very obviously different from that of a modern human or fossil hominin track. In that case, even though it is feasible to extract a 3-D "arch model" and take various measurements of it (e.g., RAV), those measurements could not be interpreted in the same ways as human track arch models, due to the vast differences between chimpanzee and human foot anatomy and kinematics. We do believe that this volumetric measurement tool is robust when analyzing the tracks of hominins who are assumed to have had foot anatomies, and to have engaged in patterns of bipedalism, that are broadly similar to those of modern humans (although the method may bring to light potentially important differences in foot kinematics). We hope that this paper provides others with the tools to carry out similar analyses of hominin tracks from sites that are already known, and from others yet to be discovered.

AUTHOR CONTRIBUTIONS

Kevin G. Hatala: Conceptualization (equal); formal analysis (lead); funding acquisition (equal); investigation (equal); methodology (supporting); project administration (equal); writing - original draft (lead); writing - reviewing & editing (equal). Peter L. Falkingham: Conceptualization (equal); formal analysis (supporting); funding acquisition (equal); investigation (equal); methodology (supporting); project administration (equal); software (equal); writing - original draft (supporting); writing - reviewing & editing (equal). Armita R. Manafzadeh: Conceptualization (equal); methodology (equal); software (equal); writing - reviewing & editing (equal). Elizabeth M. Lusardi: formal analysis (supporting); investigation (supporting); writing - reviewing & editing (equal). Stephen M. Gatesy: Conceptualization (equal); formal analysis (supporting); funding acquisition (equal); investigation (equal); methodology (equal); project administration (equal); software (equal); writing - original draft (supporting); writing - reviewing & editing (equal).

ACKNOWLEDGEMENTS

We are grateful to David Baier, Beth Brainerd, Kay Fiske, Kia Huffman, Ben Knörlein, Kyra Tani Little, Sabreen Megherhi, David North, and Morgan Turner for their assistance directly related to our biplanar X-ray experiments. We also thank the anonymous volunteers who participated in the X-ray experiments. A PRACE allocation of supercomputer resources (project 2021250007, Irene-Rome) enabled discrete element simulations. The study was supported by funding from the National Science Foundation (BCS-1825403 to K.G.H. and P.L.F.; BCS-1824821 to S.M.G.).

REFERENCES

Bennett, M. R., Harris, J. W. K., Richmond, B. G., Braun, D. R., Mbua, E., Kiura, P., Olago, D., Kibunjia, M., Omuombo, C., Behrensmeyer, A. K., Huddart, D., & Gonzalez, S. (2009). Early hominin foot morphology based on 1.5-million-year-old footprints from Ileret, Kenya. *Science*, *323*(5918), 1197–1201. https://doi.org/10.1126/science.1168132

Blickhan, R. (1989). The spring-mass model for running and hopping. *Journal of Biomechanics*, *22*(11–12), 1217–1227. https://doi.org/10.1016/0021-9290(89)90224-8

Bramble, D. M., & Lieberman, D. E. (2004). Endurance running and the evolution of *Homo*. *Nature*, *432*(7015), 345–352.

Cavagna, G. A., Saibene, F. P., & Margaria, R. (1963). External work in walking. *Journal of Applied Physiology*, *18*(1), 1–9. https://doi.org/10.1152/jappl.1963.18.1.1

Cavanagh, P. R., & Rodgers, M. M. (1987). The arch index: A useful measure from footprints. *Journal of Biomechanics*, *20*(5), 547–551. https://doi.org/10.1016/0021-9290(87)90255-7

Day, M. H., & Wickens, E. H. (1980). Laetoli Pliocene hominid footprints and bipedalism. *Nature*, *286*(5771), 385–387. https://doi.org/10.1038/286385a0

DeSilva, J. M., & Throckmorton, Z. J. (2010). Lucy's flat feet: The relationship between the ankle and rearfoot arching in early hominins. *PLoS ONE*, *5*(12), e14432. https://doi.org/10.1371/journal.pone.0014432

Domjanic, J., Seidler, H., & Mitteroecker, P. (2015). A combined morphometric analysis of foot form and its association with sex, stature, and body mass: Morphometric analysis of footprint form. *American Journal of Physical Anthropology*, *157*(4), 582–591. https://doi.org/10.1002/ajpa.22752

Drapeau, M. S. M., & Harmon, E. H. (2013). Metatarsal torsion in monkeys, apes, humans and australopiths. *Journal of Human Evolution*, *64*(1), 93–108. https://doi.org/10.1016/j.jhevol.2012.10.008

Falkingham, P. L., & Gatesy, S. M. (2014). The birth of a dinosaur footprint: Subsurface 3D motion reconstruction and discrete element simulation reveal track ontogeny. *Proceedings of the National Academy of Sciences*, *111*(51), 18279–18284. https://doi.org/10.1073/pnas.1416252111

Falkingham, P. L., Turner, M. L., & Gatesy, S. M. (2020). Constructing and testing hypotheses of dinosaur foot motions from fossil tracks using digitization and simulation. *Palaeontology*, *63*(6), 865–880. https://doi.org/10.1111/pala.12502

Hatala, K. G., Gatesy, S. M., & Falkingham, P. L. (2021). Integration of biplanar X-ray, three-dimensional animation and particle simulation reveals details of human 'track ontogeny'. *Interface Focus*, *11*(5), 20200075. https://doi.org/10.1098/RSFS.2020.0075

Hatala, K. G., Gatesy, S. M., & Falkingham, P. L. (2023). Arched footprints preserve the motions of fossil hominin feet. *Nature Ecology & Evolution*, *7*(1), 32–41. https://doi.org/10.1038/s41559-022-01929-2

Hatala, K. G., Perry, D. A., & Gatesy, S. M. (2018). A biplanar X-ray approach for studying the 3D dynamics of human track formation. *Journal of Human Evolution*, *121*, 104–118. https://doi.org/10.1016/j.jhevol.2018.03.006

Hicks, J. H. (1954). The mechanics of the foot: II. The plantar aponeurosis and the arch. *Journal of Anatomy*, *88*, 25–30.

Holowka, N. B., & Lieberman, D. E. (2018). Rethinking the evolution of the human foot: Insights from experimental research. *Journal of Experimental Biology*, *221*(17), jeb174425. https://doi.org/10.1242/jeb.174425

Holowka, N. B., Richards, A., Sibson, B. E., & Lieberman, D. E. (2021). The human foot functions like a spring of adjustable stiffness during running. *Journal of Experimental Biology*, *224*, 219667. https://doi.org/10.1242/jeb.219667

Holowka, N. B., Wallace, I. J., & Lieberman, D. E. (2018). Foot strength and stiffness are related to footwear use in a comparison of minimally- vs. Conventionally-shod populations. *Scientific Reports*, *8*(1), 3679. https://doi.org/10.1038/s41598-018-21916-7

Kelly, L. A., Cresswell, A. G., Racinais, S., Whiteley, R., & Lichtwark, G. (2014). Intrinsic foot muscles have the capacity to control deformation of the longitudinal arch. *Journal of The Royal Society Interface*, *11*(93), 20131188. https://doi.org/10.1098/rsif.2013.1188

Kelly, L. A., Lichtwark, G., & Cresswell, A. G. (2015). Active regulation of longitudinal arch compression and recoil during walking and running. *Journal of The Royal Society Interface*, *12*(102), 20141076. https://doi.org/10.1098/rsif.2014.1076

Ker, R. F., Bennett, M. B., Bibby, S. R., Kester, R. C., & Alexander, R. McN. (1987). The spring in the arch of the human foot. *Nature*, *325*, 147–149.

Kloss, C., & Goniva, C. (2011). LIGGGHTS—open source discrete element simulations of granular materials based on Lammps. In *TMS2011, 140th Annual Meeting & Exhibition, San Diego, CA, 27 February–3 March, Suppl. Proc., Vol. 2, Materials fabrication, properties, characterization, and modeling* (pp. 781–788). John Wiley.

Leakey, M. D., & Hay, R. L. (1979). Pliocene footprints in the Laetoli beds at Laetoli, northern Tanzania. *Nature*, *278*, 317–323.

McKenzie, R. T. (1909). *Exercise in education and medicine*. W.B. Saunders Company.

Morse, S. A., Bennett, M. R., Liutkus-Pierce, C., Thackeray, F., McClymont, J., Savage, R., & Crompton, R. H. (2013). Holocene footprints in Namibia: The influence of substrate on footprint variability. *American Journal of Physical Anthropology*, *151*(2), 265–279. https://doi.org/10.1002/ajpa.22276

Morton, D. J. (1924). Evolution of the longitudinal arch of the human foot. *Journal of Bone and Joint Surgery*, *6*, 56–90.

Prang, T. C. (2015). Rearfoot posture of *Australopithecus sediba* and the evolution of the hominin longitudinal arch. *Scientific Reports*, *5*(1), 17677. https://doi.org/10.1038/srep17677

Schuster, R. W., Cresswell, A., & Kelly, L. (2021). Reliability and quality of statistical shape and deformation models constructed from optical foot scans. *Journal of Biomechanics*, *115*, 110137. https://doi.org/10.1016/j.jbiomech.2020.110137

Stanković, K., Booth, B. G., Danckaers, F., Burg, F., Vermaelen, P., Duerinck, S., Sijbers, J., & Huysmans, T. (2018). Three-dimensional quantitative analysis of healthy foot shape: A proof of concept study. *Journal of Foot and Ankle Research*, *11*(1), 8. https://doi.org/10.1186/s13047-018-0251-8

Stearne, S. M., McDonald, K. A., Alderson, J. A., North, I., Oxnard, C. E., & Rubenson, J. (2016). The foot's arch and the energetics of human locomotion. *Scientific Reports*, *6*(1), 19403. https://doi.org/10.1038/srep19403

Stukowski, A. (2010). Visualization and analysis of atomistic simulation data with OVITO – the Open Visualization Tool. *Modelling and Simulation in Materials Science and Engineering*, *18*, 015012.

Tsung, B. Y. S., Zhang, M., Fan, Y. B., & Boone, D. A. (2003). Quantitative comparison of plantar foot shapes under different weight-bearing conditions. *The Journal of Rehabilitation Research and Development*, *40*(6), 517. https://doi.org/10.1682/JRRD.2003.11.0517

Venkadesan, M., Yawar, A., Eng, C. M., Dias, M. A., Singh, D. K., Tommasini, S. M., Haims, A. H., Bandi, M. M., & Mandre, S. (2020). Stiffness of the human foot and evolution of the transverse arch. *Nature*, *579*(7797), 97–100. https://doi.org/10.1038/s41586-020-2053-y

Ward, C. V., Kimbel, W. H., & Johanson, D. C. (2011). Complete fourth metatarsal and arches in the foot of *Australopithecus afarensis*. *Science*, *331*(6018), 750–753. https://doi.org/10.1126/science.1201463

Welte, L., Kelly, L. A., Kessler, S. E., Lieberman, D. E., D'Andrea, S. E., Lichtwark, G. A., & Rainbow, M. J. (2021). The extensibility of the plantar fascia influences the windlass mechanism during human running. *Proceedings of the Royal Society B: Biological Sciences*, *288*(1943), 20202095. https://doi.org/10.1098/rspb.2020.2095

Welte, L., Kelly, L. A., Lichtwark, G. A., & Rainbow, M. J. (2018). Influence of the windlass mechanism on arch-spring mechanics during dynamic foot arch deformation. *Journal of The Royal Society Interface*, *15*(145), 20180270. https://doi.org/10.1098/rsif.2018.0270

Williams, D. S., & McClay, I. S. (2000). Measurements used to characterize the foot and the medial longitudinal arch: Reliability and validity. *Physical Therapy*, *80*(9), 864–871. https://doi.org/10.1093/ptj/80.9.864

APPENDIX 1: Detailed instructions for implementing arch measurement tool in Autodesk Maya

Overview

One of our arch measurement workflows is designed for polygonal track and foot models in .obj format imported into Autodesk Maya (we developed the tool using an educational license for Maya 2022, and can confirm full functionality for Maya 2023). The source of .obj models can vary, from photogrammetry to various scanning hardware/software (laser, structured light, CT) to custom-creation within Maya (or other animation software) itself.

Basic Steps

1) Download and prepare Maya:

Autodesk Maya is available as a free trial (https://www.autodesk.com/products/maya/trial-intake) and students and educators are eligible for an annually renewable free license (https://www.autodesk.com/education/edu-software/overview?sorting=featured&filters=individual). Most of Maya's default settings are satisfactory, but two are critical to note for proper functioning of our arch measurement scripts. First, we change from a Y-up world to a Z-up world (Windows menu > Settings/Preferences > Preferences > Settings > World Coordinate System > Up axis > Z), following the convention adopted for the X-ray Reconstruction of Moving Morphology (XROMM) workflow (Brainerd et al., 2010; Knörlein et al., 2016). Second, we retain Maya's default, centimeter-based linear units (again as in XROMM). Most other software used to generate 3-D polygonal models uses millimeters or meters, so .obj's may require rescaling to produce correct results (see Step 6).

2) Download example datasets and save scripts:

In order for Maya to source these .mel files upon start-up, both need to be kept in an appropriate script folder with a filepath specific to PC and Mac operating systems. Scripts can be sourced in the Script Editor (File > Source Script) to avoid a restart, but should be stored with other .mel files thereafter.

3) Run archBooSetup1.0.mel script

The setup script is run by typing archBooSetup### into the Maya command line (set to MEL, not Python as source). This code creates a triangular prism (prism), three control locators at the vertices of the prism's base (heelLocator, mpLocatorA, mpLocatorB), a transparent yellow shader (prismShader), and hidden nodes and connections that dictate prism behavior.

4) Run archBooMaker1.0.mel script

Running archBooMaker### in the command line opens a small interface window that lets the user select a model for analysis, designate track/foot and left/right input, adjust the height of the prism, and edit the default output model name. The window's elements are described in steps 10-14.

5) Import model(s)

Track and foot .obj models can be imported by: File menu > Import/Export > Import… options > General Options > File type > OBJ. A user can also use the impObjs Data type option in the Import Data ("imp") tool that is part of the XROMM_tools shelf (https://bitbucket.org/xromm/xromm_mayatools/src/master/).

6) Scale model to centimeters

The default linear unit in Maya is centimeters. Models imported in millimeter or meter units will need to be scaled accordingly. After selecting the model, change the Scale X, Scale Y, and Scale Z values in the Channel Box to rescale.

7) Translate and rotate track model

Arches can be measured from models in any orientation and position, but track .obj's require proper alignment to yield valid pitch, roll, and relative depth results. For most track models, the user will likely need to use the translate and rotate manipulators to set the undisturbed ground surface at the horizontal (XY) plane. Modifying the model's pivot (Modify menu > Pivot > Center Pivot), showing the grid in each camera (Show > Grid), and using the four pane view can make track manipulation easier.

8) Check and fix normals

In order for the arch Boolean to calculate correctly, the face normals of the track or foot model must point in a predictable direction. Our scripts require the normals of a track .obj to point upward from the top (+Z) surface of the model. A foot .obj should have its normals pointing outward from the external surface of the model. If Maya's default lighting is used (Two Sided Lighting off), the lower surface of a track model and inner surface of a foot model should appear black. To check the normals visually, toggle them on by selecting: Display menu > Polygons > Face Normals. Normals can be flipped by first choosing the Modeling menu set, then selecting: Mesh Display menu > Normals > Reverse.

9) Place landmark locators

Select the model that you wish to measure, then make it a live surface (Modify menu > Objects > Make Live). Select a locator, choose the Translate tool, and drag it to its appropriate position on the model that you are measuring. Note that we have designed the tool such that the heelLocator should be placed at the center of the heel impression and, if you are measuring a right track or foot model, mpLocatorA will be at the impression beneath the first metatarsophalangeal joint and mpLocatorB at the impression beneath the fifth metatarsophalangeal joint. If you are measuring a left track or foot model, then the positions of the latter two will be reversed (mpLocatorA at the fifth and mpLocatorB at the first metatarsophalangeal joint).

In the Calculate Arch Boolean window:

10) Select the appropriate track/foot model for measurement

Select the model that you are measuring, and click "Insert" next to the "Model" field.

11) Designate the type of model and its side

Use the toggle buttons to select the appropriate combination of track/foot and right/left.

12) Adjust prism height

If necessary, use the slider or the text box to adjust the height of the prism, such that it exceeds the height of the arch you are measuring. Note that the prism cannot be too tall, such that it penetrates through overhanging features of a track model, or through the dorsal side of a foot model.

13) Edit default name of arch boolean

If desired, change the name of the arch boolean - this will become the name of the arch model extracted from the track/foot that you are measuring.

14) Click Calculate and Measure Arch Boolean button

The script will perform the Boolean operation, and will compute the designated measurements of the arch model (see Table 1 for descriptions). Note that some variables may be irrelevant to the type of arch that you are measuring. For example, when measuring a foot model the script will still output mid-axis depth, relative depth, pitch, and roll, which are irrelevant for an object that is not aligned to a particular global coordinate system.

15) Output products/effects

After running the Boolean, you will see a red arch model with keyed data that includes the relevant measurements of that model.The prism and the track/foot model will be automatically hidden. The translations (i.e., positions) of the locators will also be keyed, such that you retain a record of where they were placed for a given measurement.

16) Measuring the next model

When continuing on to measure a subsequent model, use the existing locators, prism, and interface window (do not run the scripts multiple times). Be sure to advance the animation frame, in order to avoid overwriting your keyed locator positions, and unhide the locators and prism. Once you have done this, you can repeat Steps 5-16 for as many models as desired.

17) Exporting measurements

There are multiple ways to export arch model measurements from Maya. Perhaps the simplest is to copy and paste values from the Channel Box/Layer Editor immediately following each measurement. However, we prefer to use the Export (‘exp’) function that is part of the XROMM_tools shelf (https://bitbucket.org/xromm/xromm_mayatools/src/master/). By shift-selecting all arch models, and all measurement attributes from the Channel Box/Layer Editor, pressing the ‘exp’ button and choosing the ‘Selected attributes’ option, one can export a single Excel file that contains measurements of all keyframed arch objects.

Variables and conventions

Keyed on arch model:

Relative Arch Volume cube root volume divided by ⅔ root base area, expressed as a %

Relative Depth	depth of arch axis at midpoint divided by arch axis length
Pitch	pitch of arch axis in degrees (heel deeper positive)
Roll	roll of mp axis about arch axis in degrees (external positive)
Arch Volume	volume of arch Boolean in cm3
Base Area	area of prism base in cm2
Axis Length	length from heel to middle of mp-axis in cm
Mid Axis Depth	depth of arch axis mid-point in cm
Side	right or left foot selected

Keyed on prism base locators:

XYZ coordinates

APPENDIX 2: Detailed instructions for implementing arch measurement tool in Blender

Overview

This appendix details the use of the arch measurement tool in Blender. The tool works on polygonal meshes, which may be imported as obj, stl, ply etc, and can be sourced from various scanning hardware (photogrammetry, laser scanning, CT etc).

Basic steps/setup

Download blender and install the extension:

Blender is free and open source, and is available from www.blender.org for Mac, Windows, and Linux. It can also be compiled from source. Multiple control schemes are available, but whether you use blender, industry standard, or custom commands, there should be no conflicts with the arch measurement tool. Default blender settings should work fine, but ensure scene scale is set appropriately, and that foot/track models match this.

Download the latest release of the extension from: https://github.com/pfalkingham/ArchBooBlender/releases/ . The release is downloaded as a small zip file.

To install the extension, in blender go to edit->preferences->addons and click 'install', then enable the addon if it is not enabled by default.

The process should work on track/foot models in any orientation, but it is best practice to align models such that the tracking surface is at z=0 and aligned with the xy plane.

Tracks should have normals pointing upwards, and feet should have normals pointing outwards. If they do not, you can flip normal using blender.

Using the addon

Once the addon is successfully installed and enabled, a new tab will appear in the 3D viewport on the right, called 'ABM'.

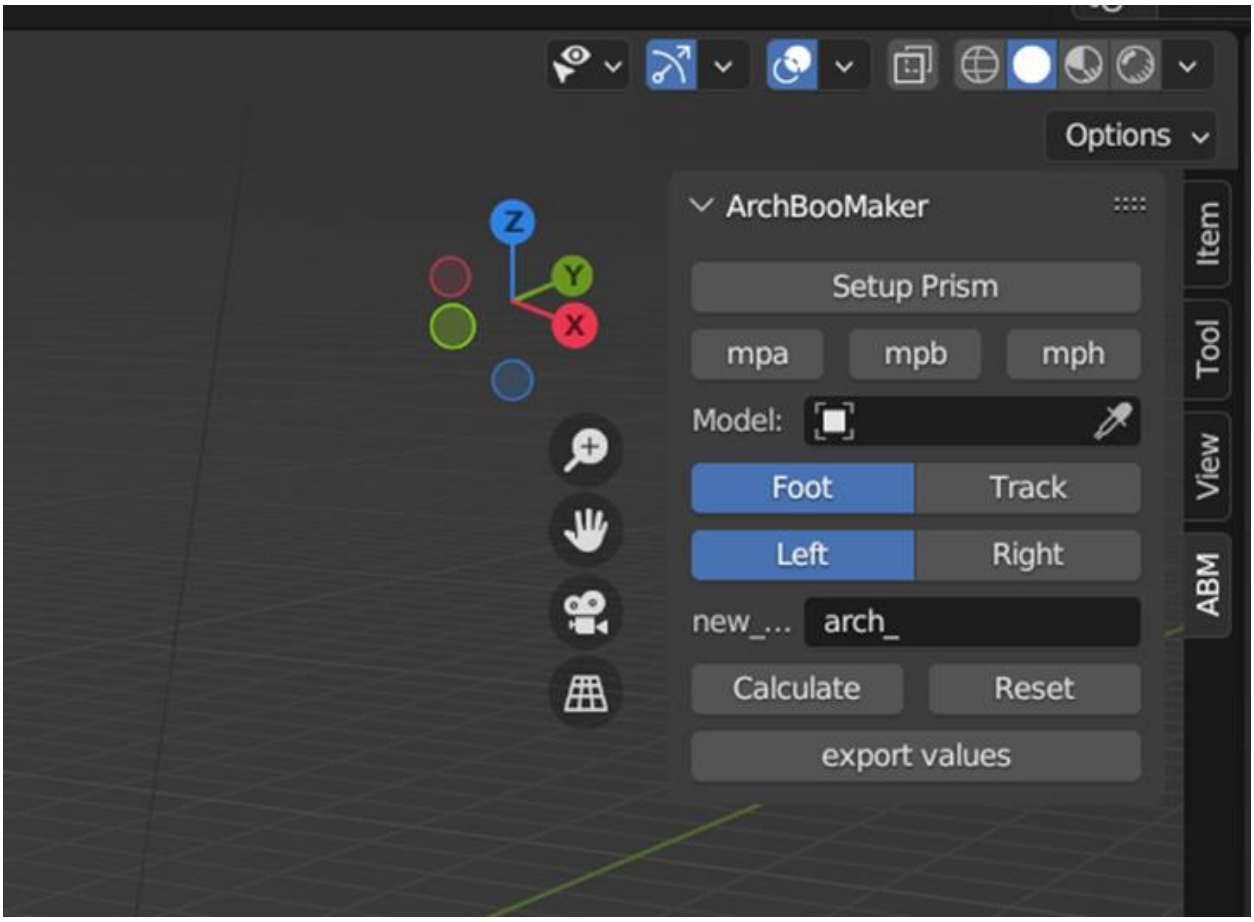

1. Click ‘Setup Prism’ to generate the prism and locators that will define the arch.

2. Move the locators mpa, mpb and mph in the viewport. The locators can be selected in the viewport, or the three buttons ‘mpa’, ‘mpb’, and ‘mph’ can be used to quickly select them. We suggest using blender’s ‘snap to vertex’ function to ensure the locators are on the foot/track model surface.
If the foot or track is a right, mpa should sit in the base of the 1st metatarsal head [impression] and mpb should sit in the 5th metatarsal head[impression]. A ‘left’ track/foot would need mpa and mpb reversed. ‘mph’ should be be positioned in the centre of the heel.

3. Select the foot or track model – this can be done by clicking within the ‘model’ field of the ABM UI, or using the eyedropper tool to select the object in the viewport.

4. Select whether the model is a foot or a track

5. Select whether it is of a left or right foot or track.

6. The name box specifies the prefix – the generated arch model will take the name of the foot or track model, prefixed by what is in this box (*It is strongly recommend leaving as default ‘arch_’ such that a model ‘track1’ results in an arch object called ‘arch_track1’*)

7. If necessary, ensure that the prism object rises above the tracking surface, or is short enough to not extend out the dorsal surface of a foot model, using a custom property in the prism object properties.

8. Click the ‘calculate’ button to create an arch object.

9. The resultant arch object contains all relevant calculation data as custom properties:

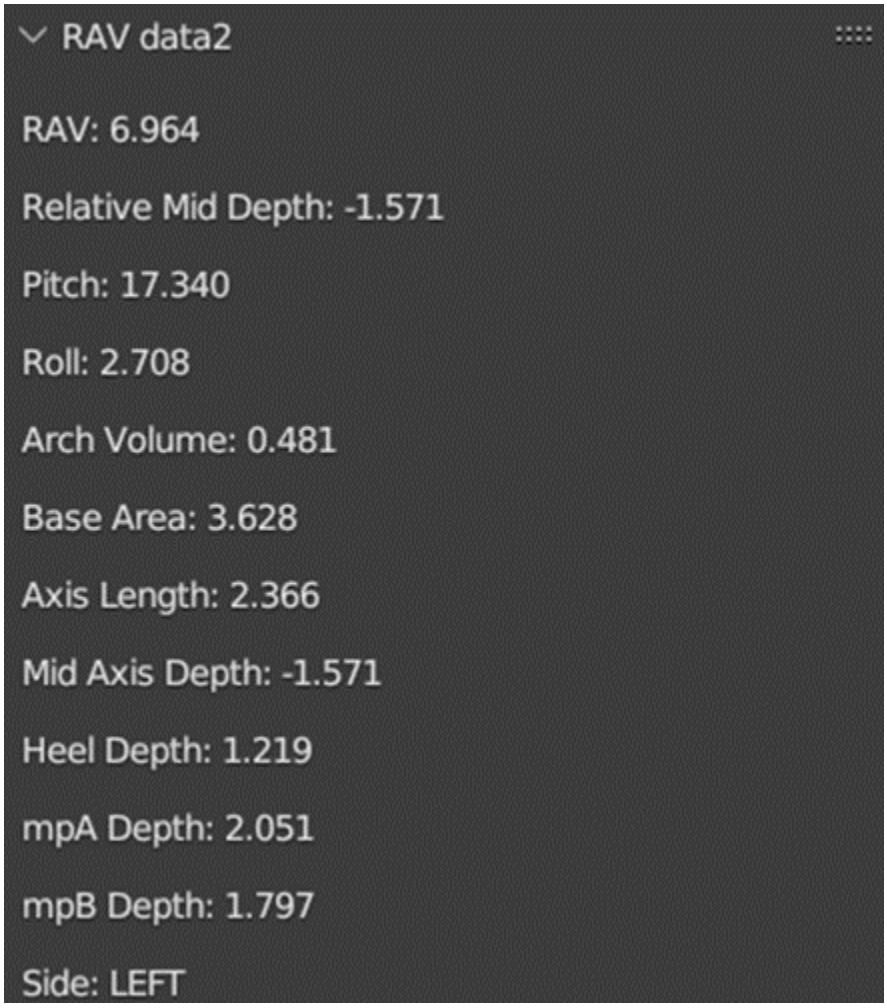

10. The ‘export values’ button will export all calculated values from all arch_* objects in the scene to a csv file in a location of the user’s choosing. *Note that at time of writing this is hard-coded only to export arch_* objects, so if a custom prefix was used, this function will not work.*

At any point, the ‘reset’ button will delete the prism and locators, and recreate them. This can be useful if mistakes are made, or something goes wrong.